


# Experimental and Numerical Study on Tapping of Two Liquids through a Single Tap-Hole

Varun LOOMBA,<sup>1)</sup> Jan Erik OLSEN,<sup>2)\*</sup>  Quinn Gareth REYNOLDS,<sup>3,4)</sup> Oliver OXTOBY<sup>5)</sup> and Kristian Etienne EINARSRUD<sup>1)</sup>

1) Department of Materials Science and Engineering, Norwegian University of Science and Technology (NTNU), Trondheim, 7491 Norway.

2) SINTEF, Trondheim, 7465 Norway.

3) Mintek, Randburg Johannesburg, 2125 South Africa.

4) Stellenbosch University, Matieland Stellenbosch, 7602 South Africa.

5) ENGYS, SW18 3SX, London, UK.

(Received on April 25, 2023; accepted on August 23, 2023)

The production of industrial metals in pyrometallurgical smelting furnaces is central to modern industry. Tapping of metal and slag from smelting furnaces is a complex and difficult process. Any variations from tap to tap reduce predictability and impact the planning of downstream logistics. Tapping of metal and slag can be generalized as drainage of two immiscible liquids through a particle bed. In the present paper this is studied by both laboratory experiments and numerical modeling of water and oil drainage from a tank. The results show that the numerical model and physical experiment are consistent. This provides confidence that the numerical models can be applied to quantify tapping from metallurgical furnaces.

KEY WORDS: tapping; modelling; experiment; CFD.

## 1. Introduction

In the majority of metallurgical furnaces, process products such as metal and slag are extracted through a tap-hole in the molten state. This applies to blast furnaces, submerged arc furnaces (SAF) and electric arc furnaces (EAF). Slag is generally a by-product or waste, with the metal being the product of value. In many of these furnaces the immiscible metal and slag phases are tapped through a single tap-hole<sup>1)</sup> close to the bottom of the furnace as shown in Fig. 1. Some furnaces are tapped continuously with a semi-permanent open tap-hole, whereas others are tapped discontinuously with a given frequency by closing and opening the tap-hole.<sup>2)</sup> Iron and ferroalloys such as ferromanganese (FeMn), silicomanganese (SiMn) and ferrochromium (FeCr) are typically tapped discontinuously through a single tap-hole together with slag.<sup>3)</sup> In principle this is a straightforward operation, but the quantity of products extracted, the flow-rate of the tapping stream, and the relative fraction of metal and slag can vary appreciably from tap to tap. The tapping process is also sometimes delayed or stopped due to blockages in the tap-hole channel or other operational problems. This variability causes upsets in furnace inventory which affect metallurgical performance and later taps, and

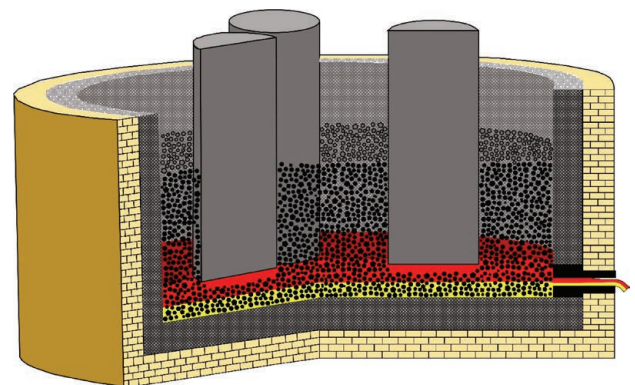


Fig. 1. Illustration of tapping from a submerged arc furnace. (Online version in color.)

can directly affect the logistics of downstream operations. Excessive unpredictability in the tapping process may also create hazardous situations for the furnace operators. There is therefore an interest in improving knowledge and understanding of the tapping process.

The metal (or alloy) and slag in ferroalloy processes are generally produced inside submerged arc electric smelting furnaces by carbothermic reduction of metal-bearing ores. This process continuously increases the amount or level of products inside the furnace over time. The levels are reduced

\* Corresponding author: E-mail: Jan.E.Olsen@sintef.no



when the tap-hole is opened and the material is allowed to drain out of the vessel. During tapping the liquids have to flow through the furnace burden, a packed bed of particles consisting of ore and carbonaceous reductants such as coke or coal. The particle bed causes a resistance to the tapping flow towards the tap-hole, especially close to the outlet where the liquids are accelerated to converge into the narrow tap-hole channel.<sup>4)</sup> Being able to understand how the particle bed affects the tapping process is important, and concerns understanding flow phenomena which occur when multiple immiscible liquids drain through a porous medium such as a particle bed. This is not only relevant in metallurgical operations but also in other industries such as the petroleum (where oil-water flow is one of the most commonly encountered problems), and the chemical and process industry (where packed bed reactors are applied extensively for single or multiple fluid reactions, e.g.<sup>5,6)</sup> Insight on this phenomenon can be extracted from both experimental studies and numerical models.

Several experimental studies on liquid drainage through a particle bed under laboratory conditions have been conducted. This includes the work by Fukutake and Okabe<sup>7)</sup> on experiments in a cylindrical vessel with glass beads with a single viscous fluid to emulate the flow of slag in the industrial scale furnaces, Luomala *et al.*<sup>8)</sup> on the flow of water through a particle bed, Vango *et al.*<sup>9)</sup> on the drainage of a water through a particle bed under both settled and floating bed conditions, Liang *et al.*<sup>10)</sup> on water being drained from the bottom of a rectangular tank with both open and closed top surface, and Zhang *et al.*<sup>11)</sup> on the drainage of water through a floating particle bed with rotational and translational oscillations. Most of this research studied drainage effects using a single liquid only. To the authors' knowledge, there are relatively few studies that have considered the flow of multiple fluids through a particle bed. Tanzil *et al.*<sup>12)</sup> and Liu *et al.*<sup>13)</sup> performed experiments with two immiscible fluids in a Hele-Shaw physical model, a 2D model with two parallel plates placed close to each other with particle bed inside it. The interface behavior in a 2D and a 3D environment is substantially different, therefore care must be taken while analyzing the results. He *et al.*<sup>14)</sup> focused on the interfacial behavior of two immiscible fluids passing through a particle bed in both 2D (Hele-Shaw) and 3D (cylindrical vessel with particles inside) arrangements, with a focus on movement of the gas-liquid interface. Nouchi *et al.*<sup>15)</sup> examined a two-phase flow using fluoride fluid and liquid paraffin under different particle bed conditions, concentrating on the flow rates of each fluid. Loomba *et al.*<sup>16)</sup> performed laboratory-scale drainage experiments with two fluids through a particle bed, focusing on the change in the tapping rates over time due to the presence of the particle bed.

Extensive work has been done in the development and application of numerical models to the study of furnace tapping. Several researchers have implemented computational fluid dynamics (CFD) models to determine the flow profiles of the metal and the slag in the hearth of the furnace during tapping. Numerical simulation permits easy modification of structural parameters such as the design of the furnace or the shape of the tap-hole,<sup>17)</sup> size of the particles and particle bed packing,<sup>18)</sup> and the effect of the pressure near to the electrode tips.<sup>19)</sup> Other researchers have applied Bernoulli's equation describing the flow along a flowline

for an inviscid flow.<sup>15,20,21)</sup> This introduces more approximations and empirical parameters into the model, but reduces the simulation time considerably compared to CFD models. The Bernoulli equation was extended to include the effect of friction, the internal furnace pressure, and the flow resistance from the particle bed. In some work the metal and the slag are not considered as separate phases, but as a mixture instead.<sup>22)</sup> To better separate between the tapping of metal and slag, Olsen and Reynolds<sup>23)</sup> treated the phases separately to permit prediction of separate slag and metal tapping rates. A more extensive review on numerical models on furnace tapping is provided by Bublik *et al.*<sup>24)</sup>

In this study we present both a laboratory-scale experiment and CFD models for drainage of two immiscible liquids through a particle bed. Results from the CFD studies are compared to the experimental test data as well as each other for consistency between the models.

## 2. Experimental Set-up

An experimental rig was set up to study the effect of a particle bed on the tapping rates of both a single liquid and two immiscible liquids. The rig consists of a plexiglass tank of dimensions  $1 \times 0.5 \times 0.6$  m. A tap-hole with a square cross section of dimensions  $0.02 \times 0.02$  m was drilled at a height of 0.03 m above the base of the tank, and was connected to an outlet channel of 0.11 m in length having the same internal dimension as the tap-hole. A similar rig was used in an earlier study<sup>16)</sup> with the tap-hole located at a different height. The end of the outlet channel was fitted with a detachable plug. At the beginning of each experiment, the plug was opened, and the liquids were allowed to drain out of the tank. The tapped liquids were collected in a bucket placed on an OHAUS Defender 5000 weighing scale (OHAUS New Jersey, USA). The scale recorded the total weight of tapped liquid each second. A high-speed camera (Sony Cybershot DSC-RX10 IV, Japan) was positioned in front of the tank to capture the moving interface between the two liquids as they were tapped. The test rig is shown in **Fig. 2**.

### 2.1. Liquids

Metal and slag are immiscible liquids, with the denser metal forming a layer below the lighter slag. To emulate the flow properties of metal and slag at room temperature water and a mineral oil with physical properties shown in **Table 1** were used. Interfacial tension between all phases was set to 0.07 N/m. The choice of liquids was not based on scalability of the process, but on the potential of validating numerical models which can be used to better understand the scaled-up process. In particular, liquids with properties resulting in a bend of the interface towards the tap-hole was targeted. The mineral oil was chosen such that its density is lower than water and is at least 20 times more viscous than water. For comparison some values for metal and slag from FeMn smelting processes at typical furnace operating conditions<sup>3)</sup> are also shown in Table 1. **Figure 3** shows the two immiscible fluids at the beginning of the experiment, where oil forms the upper layer and water the lower layer. Since the oil and water are both colorless liquids, a water-soluble food coloring was added to the water to distinguish the interface between the phases in the video.

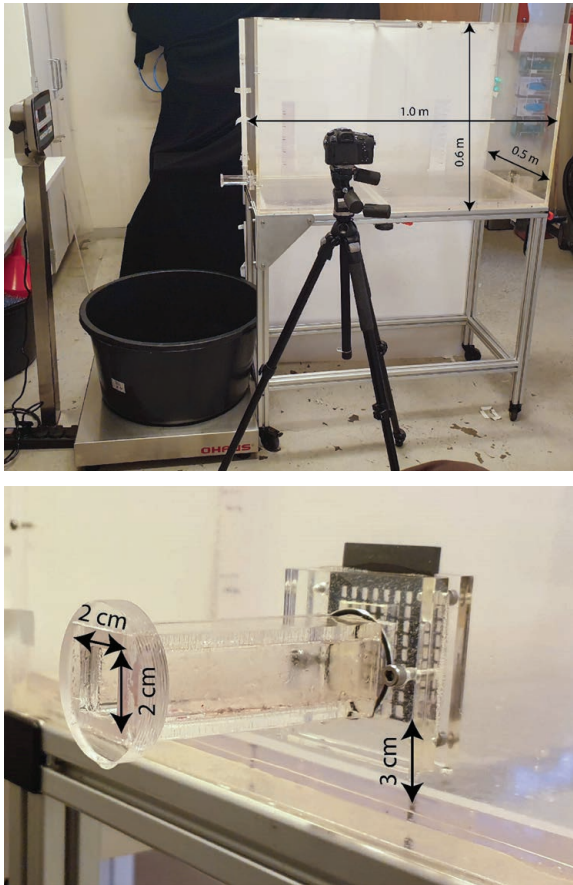


**Fig. 2.** (top) Experimental test rig including the plexiglass tank of dimension  $1 \times 0.5 \times 0.6$  m, a high-speed digital camera and a weighing scale, (bottom) Close-up of the tap-hole and outlet channel. (Online version in color.)

**Table 1.** Physical properties of fluids.

Material	Density (kg/m <sup>3</sup> )	Viscosity (kg/m-s)
Water	1 000	0.001
Mineral Oil	876	0.057
FeMn	6 100	0.005
Slag	3 000	0.1

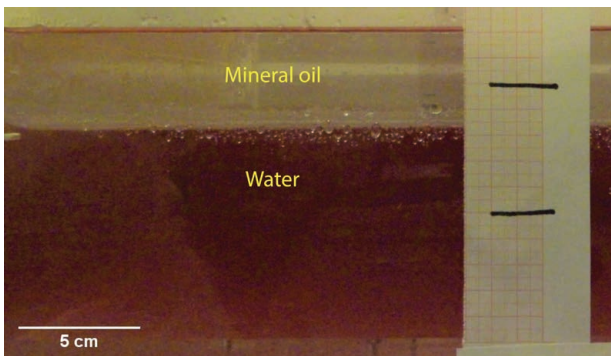


**Fig. 3.** Image of water and oil phases in the tank (without particle bed). (Online version in color.)

## 2.2. Particle Bed

The presence of a particle bed in a furnace reduces the tapping flowrate, as it induces a pressure drop across the bed

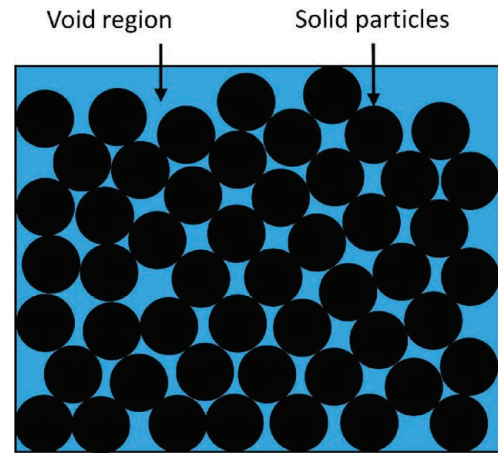


**Fig. 4.** Schematic diagram of particle bed porosity. (Online version in color.)

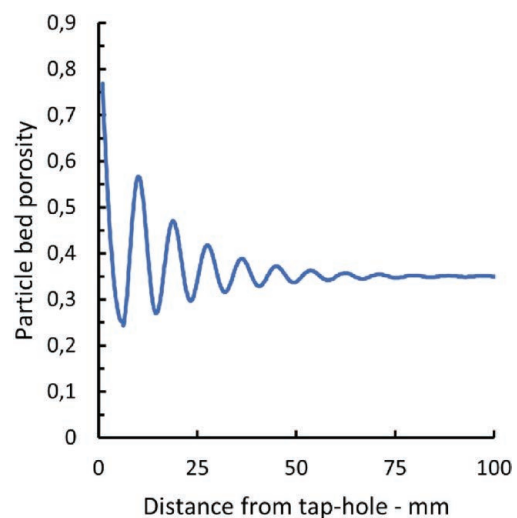


**Fig. 5.** Plot of particle bed porosity as function of distance from tap-hole for 10 mm particles. (Online version in color.)

due to the resistance offered by the particles to the moving fluid. Spherical glass particles of 0.01 m diameter were used to emulate the burden particle bed in the furnace. A mesh was placed in front of the tap-hole interface to prevent the particles from moving out of the tap-hole. The mesh was coarse enough not to provide any significant resistance to the flow of liquids,<sup>16)</sup> but fine enough to act as a wall for the particles. A particle bed can be defined by two of its properties, the particle diameter,  $d_p$ , and the particle bed porosity  $\epsilon$ . The porosity is defined as the ratio of the void volume to the complete volume of the confined space without the particles.

**Figure 4** shows a 2D schematic diagram depicting the porosity of a particle bed. Generally, randomly packed mono-sized particle beds have a porosity in the range 0.35–0.5.<sup>25)</sup> The porosity of the particle bed in the tapping tank experiment was measured by adding a known amount of water to the tank, measuring the height, and comparing it with volume without the particles. The value was found to be approximately 0.35. Close to walls the porosity deviates from the bulk value since the walls reduce the freedom of particles to pack closely. de Klerk<sup>26)</sup> derived a correlation for the particle bed porosity as function of distance from the wall - this effect is seen in **Fig. 5**.

**2.3. Image Analysis**

A limitation of the weighing scale is that it is only able to record the total mass of liquid tapped. The mass of individual phases cannot be determined from the weight alone. Therefore, video captured by the camera was analysed to calculate the tapping rates of the individual phases. Screenshots were taken from the video at specific time intervals and the position of the interfaces was determined using the Image Analysis Toolbox of MATLAB® 2019b. These interface heights were used to calculate the volume, and hence the mass, of each phase inside the tank at any instant, and these values were subtracted from the initial masses to estimate the tapped mass.

**2.4. Methodology**

The aim of these experiments was to understand the effect of the particle bed on the tapping rates of two immiscible fluids under various combinations of conditions. Therefore, several experiments were conducted with water and oil in the presence and absence of a particle bed, to understand its effect. The first experiment was performed without any particle bed and only a water phase (Exp 1). In the second experiment, oil phase was added together with water to study its effect on the tapping rates (Exp 2). The particle bed was then added once these experiments were completed. The next two experiments were performed with only water in the tank, the first (Exp 3) with the same volume of water as in Exp 1, and the second with the same height as the height of the particle bed (Exp 4). Finally, experiments with both water and oil volumes as used in Exp 2 were performed (Exp 5). The details of all the experimental conditions are summarized in **Table 2**. It should be noted that while performing multiple repeats with water and oil in the presence of the particle bed, oil would contaminate the surface of the glass beads, and air bubbles would also get trapped between the particles in the bed. These issues were difficult to avoid while refilling the tank for successive experiments (each experiment was performed with 4 repeats). The average of the repeats for each experiment are reported below. There were less than 3% deviation between the repeats.

**3. Numerical Model**

A numerical model based on CFD methods was set up to simulate the flow of the two immiscible liquids. CFD solves conservation equations for mass and momentum to obtain fluid velocities and pressure mathematically. With two immiscible liquid phases and a gas phase present, it is also

necessary to track the location of the interfaces between the liquids and between the top liquid and the gas above. This was done by applying the Volume of Fluid (VOF) multi-phase flow method,<sup>27)</sup> in which a single continuum equation is solved for all phases while tracking the position of each phase with a volume fraction marker field  $\alpha$ . The following differential equations are solved:

$$\nabla \cdot U = 0 \dots\dots\dots (1)$$

$$\frac{\partial(\rho U)}{\partial t} + \nabla \cdot (\rho U U) = -\nabla p + \nabla \cdot (\mu \nabla U) + \rho g + S_k \dots (2)$$

$$\frac{\partial \alpha_i}{\partial t} + (U \cdot \nabla) \alpha_i = 0 \dots\dots\dots (3)$$

Here  $U$  is the mean velocity shared by all liquid phases,  $\alpha_i$  is the individual phase volume fraction,  $\rho$  and  $\mu$  are the mixture density and viscosity,  $g$  is the gravitational acceleration acting on the fluids and  $S_k$  is a source term including interfacial tension and any other force that affects the flow. The mixture properties are given by the local volume fraction of the phases. For example, the mixture density is given by the following expression:

$$\rho = \sum \alpha_i \rho_i \dots\dots\dots (4)$$

The volume fraction marker fields are constrained by

$$\sum \alpha_i = 1 \dots\dots\dots (5)$$

where  $i$  is the index of the fluid phases only. The volume of the particles is not accounted for in these equations. Thus the continuity equation, Eq. (3), neglects the presence of the particle bed and the true total volume and total mass of the liquids is adjusted in post-processing of the results. Since a particle bed is present, its resistance to the flow needs to be accounted for. This is done by defining the particle bed as a porous zone. In a porous zone the particle bed adds a resistance to the flow through the source term  $S_k$  in Eq. (2) which incorporates a correlation for the pressure loss through a particle bed. For monodisperse particle beds (or particle beds where an effective particle diameter gives a good representation of the particles), Ergun's equation<sup>28)</sup> was applied for the pressure loss

$$\nabla p = -\frac{150(1-\epsilon)^2 \mu \bar{U}}{\phi^2 d_p^2 \epsilon^3} \bar{U} - \frac{1.75(1-\epsilon) \rho}{\phi d_p \epsilon^3} |\bar{U}| \bar{U} \dots\dots\dots (6)$$

Here  $\epsilon$  is the particle bed porosity,  $d_p$  is the particle diameter and  $\phi$  is the particle sphericity. All of these can

**Table 2.** Experimental details.

Experiment	Water height (m)	Oil height (m)	Particle diameter (m)	Bed height (m)	Porosity	Total water (kg)	Total oil (kg)	Liquids above tap-hole (kg)	Tapped after 100 sec (kg)
Exp 1	0.13	-	-	-	-	65.0	0.0	50.0	32.3
Exp 2	0.09	0.04	-	-	-	45.0	17.5	30.0	25.5
Exp 3	0.22	-	0.01	0.17	0.35	54.8	0.0	49.5	25.5
Exp 4	0.17	-	0.01	0.17	0.35	29.8	0.0	24.5	16.6
Exp 5	0.18	0.04	0.01	0.17	0.35	34.8	17.5	45.3	22.7

be specified as a function of position by giving a specified value for each computational cell. Since the presence of the particles are not modelled directly as voids in the fluid domain, capillary forces between the particles are neglected. In this construct, the velocity  $U$  becomes a superficial velocity. This set of Eqs. (1)–(6) is solved together with pressure boundary conditions, material properties according to Table 1, and initial conditions according to Table 2. Wall adhesion is neglected in these cold experiments, but should be considered when addressing high temperature conditions. The model was run in two different CFD codes to identify any discrepancies due to numerical methods and software implementations. The chosen codes were OpenFOAM<sup>®</sup> and Ansys Fluent.

The simulations in Ansys Fluent were run with version 2020 R1 with a first order implicit transient formulation, the pressure implicit with splitting of operators (PISO) scheme for pressure-velocity coupling, and the Geo-Reconstruct method for interface tracking. The time step was constant at 0.001 s which kept the Courant number below 0.5. The equations were solved on a computational mesh as seen in Fig. 6. The symmetry of the tank was applied to reduce the mesh size to approximately one million cells. The resolution is finest in and close to the tap-hole with a characteristic element size of 2.5 mm.

The simulations in the OpenFOAM<sup>®</sup> open-source computational mechanics framework were conducted using ESI OpenFOAM<sup>®</sup> version 2206.<sup>29)</sup> A third-party family of solvers developed for multiphase flow problems in porous media was used.<sup>30)</sup> This solver addresses issues related to numerical stability and accuracy in regions of high porosity gradients by applying a porosity-aware formulation of the transport equations with a specialised flux limiter for the divergence terms.<sup>31)</sup> A first-order time implicit formulation was used for the transient terms, together with a standard iterative segregated solution scheme, PISO-SIMPLE, for the velocity-pressure coupling in the momentum equations. The multidimensional universal limiter for explicit solution (MULES) scheme was used for interface capturing. Adaptive time-stepping with a Courant number limit of 0.5 was applied in all cases. Computational meshes were shared with

the Fluent simulations via OpenFOAM<sup>®</sup>'s integrated mesh import and conversion tools.

#### 4. Results

Experiment 1 with no particle bed and no oil (only water) served as a reference case for the other experiments to be compared against. From the measured tapping weight after 100 seconds, we see that the tapping rate is reduced if some of the water is replaced with oil as in Experiment 2. This is consistent with the reduced pressure head due to the lower density of oil compared to water. When particles are added, we see from Experiments 3 and 4 that drainage and tapping is slowed down significantly compared to Experiment 1 without particles. This holds both for when the same water volume is tapped (Experiment 3) and for a more comparable water level (Experiment 4).

For Experiments 2, 4 and 5 numerical simulations were also performed. In Experiment 2 (see Table 2) both water and oil were tapped out of the tank without any particles present. The initial height of water was 9 cm, with a 4 cm layer of oil on top the water. During the initial stages, only water was tapped. As the interface between water and oil moved closer to the level of the tap-hole, some oil started to become entrained with the water. Towards the end of the experiment, only oil was being tapped. In Fig. 7 we see the results from a numerical simulation of the experiment at the point at which water and oil have both entered into the tap-hole, but the oil has not yet started flowing out of the tap-hole. Note how the interface between water and oil is deformed near to the tap-hole – this allows oil to be tapped well before the average level of oil in the tank reaches the height of the tap-hole. As mentioned above, being able to produce such a bend of the interface was a target when choosing the liquids.

Quantitative results from the experimental tests and the numerical simulations are seen in Figs. 8 and 9. In Fig. 8 the total tapped mass (*i.e.* the combined mass of water and oil) is plotted as function of time. By comparing the experimental results from the weighing procedure and the image analysis, we can conclude that the two measurement techniques are consistent with each other. The simulation

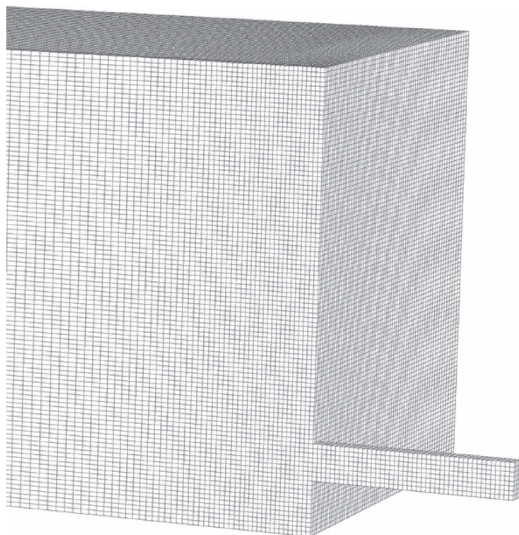


Fig. 6. Computational Mesh.

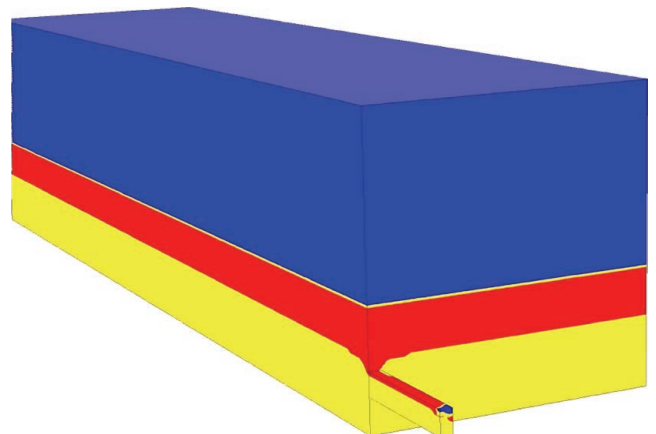
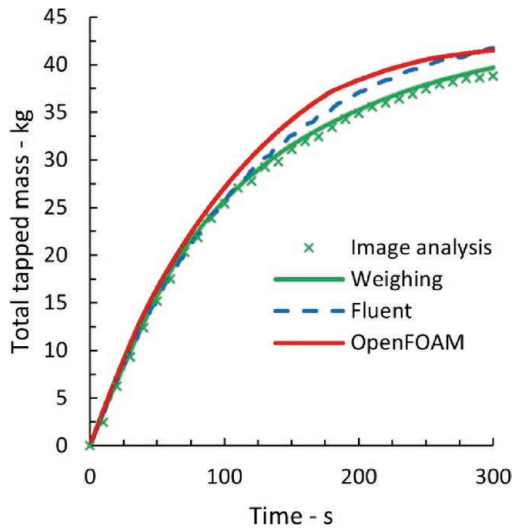
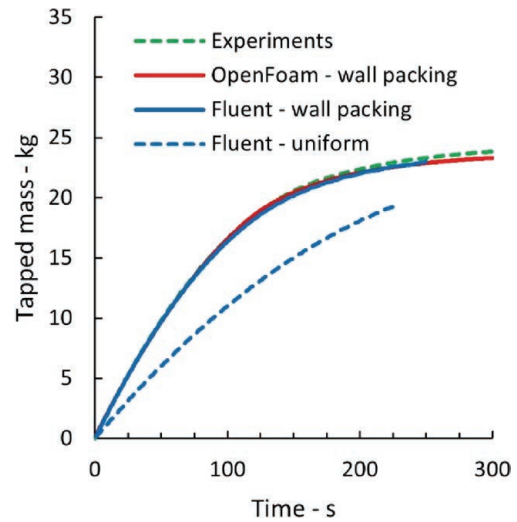


Fig. 7. Ansys Fluent numerical simulation of Experiment 2, with no particle bed present - water (yellow) and oil (red) in tank after 50 s. (Online version in color.)



**Fig. 8.** Total tapped mass in tank without particles as function of time from Experiment 2 and numerical simulations. (Online version in color.)



**Fig. 10.** Tapped mass in tank with water and particles as function of time from Experiment 4 and numerical simulations. (Online version in color.)

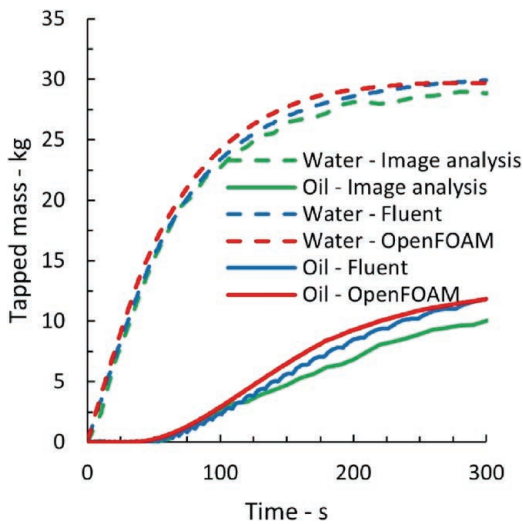


**Fig. 9.** Tapped mass of water and oil in tank without particles as function of time from image analysis of Experiment 2, and simulations. (Online version in color.)

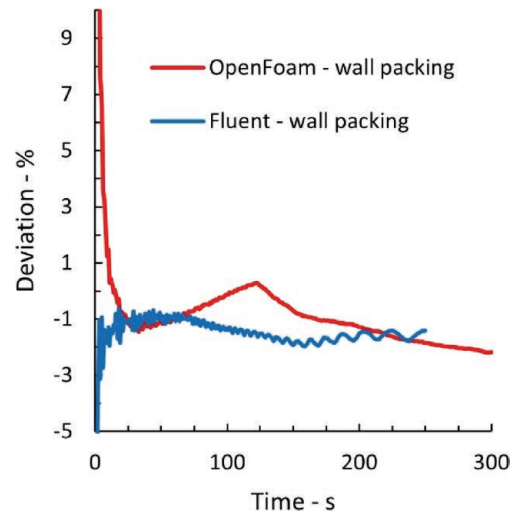


**Fig. 11.** Deviation of numerical results from experimental results. (Online version in color.)

results are consistent with the experimental results until tapping of oil is initiated. Thereafter the numerical simulations appear to slightly overpredict the oil tapping rate, although the qualitative shape of the curves and time of onset of oil tapping are similar. Over time, this accumulates to a significant deviation between experimental and numerical predictions. This may be due to poor prediction of the pressure loss in the tap-hole entry region, which might be linked to turbulence, surface roughness or surface wetting.

In Experiment 4 the tank was filled with glass beads to 17 cm above the bottom of the tank, and with water up to 17 cm. No oil was present. Water was tapped through the tap-hole and the weight of the tapped water was recorded. No image analysis on the height level was performed since only one liquid phase was present. The tapped water mass as function of time for experiments and simulations is plotted in **Fig. 10**. Here the bend of the interface is even more pronounced. The results show that numerical simulations, both with OpenFOAM<sup>®</sup> and Ansys Fluent, are consistent

with the experimental recording provided that wall packing effects are accounted for. The wall packing was accounted for by making the packing porosity a function of the distance from the wall. The resolution of the computational grid was sufficient to directly utilize the expression of Eq. (6). Without wall packing, the resistance from the particle bed is overpredicted and the tapping rate is significantly underpredicted. This agrees with recent work which shows that tapping rates are sensitive to the particle packing close to the entrance to the tap-hole.<sup>4)</sup> Here the wall packing effect is particularly important, since it can be assumed that wall packing also applies in front of the tap-hole entrance due to the mesh preventing the particles from escaping. **Figure 11** shows the deviation of the numerical simulations from the experimental results. There are some differences between OpenFOAM<sup>®</sup> and Ansys Fluent, particularly in the initial stages of the simulation. This is probably due to differences in numerical schemes and parameters. However, the total deviation is very small for both software packages. Note also that the tapping flowrate with a particle bed (Experi-

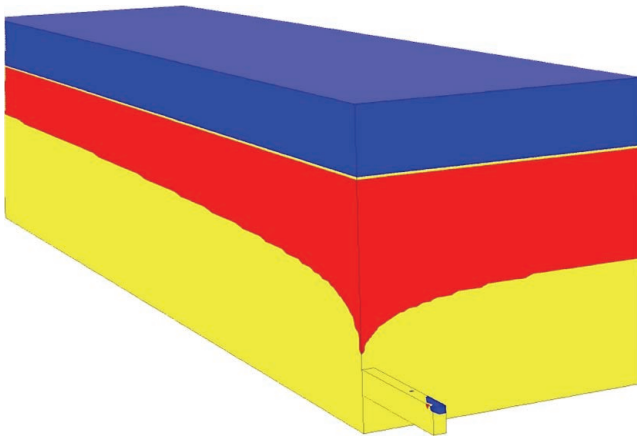


**Fig. 12.** Ansys Fluent simulation of Experiment 5, with a 17 cm particle bed - water (yellow) and oil (red) in tank after 50 secs. (Online version in color.)

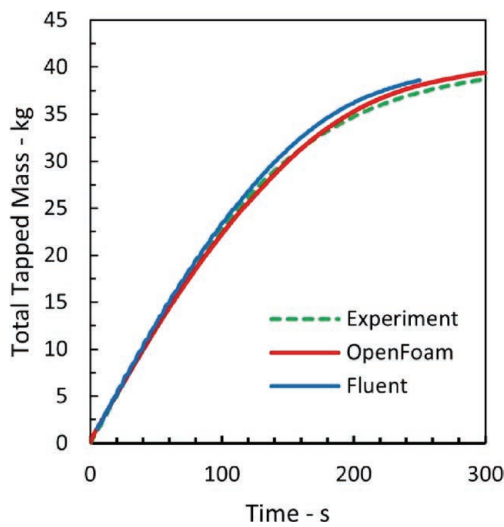


**Fig. 13.** Total tapped mass in tank with particles, water and oil as function of time from Experiment 5 and numerical simulations. (Online version in color.)

ment 4, Fig. 10) is much lower than without a particle bed (Experiment 2, Fig. 8). This indicates that the drag from the particle bed has a dominant effect on the total pressure loss through the system, and when a particle bed is present the exact prediction of pressure loss through the tap-hole channel of less importance than understanding the disposition of the particle bed just inside it.

In Experiment 5 a particle bed was again present up to 17 cm above the bottom of the tank, water up to 18 cm, and oil another 4 cm above the water. While the image analysis performed well in Experiment 2 without particles, it was not possible to properly obtain the height level of the interface between water and oil in the same way in Experiment 5 due to the reflective behavior of the particles. Still, it was possible to observe from the video photography the point in time when oil started to flow into the tap-hole - this was between 50–55 secs after tapping started. The same timing was predicted by both of the numerical simulations. Note that flow of oil out of the tap-hole is a bit delayed from when it enters the tap-hole since the oil front moves slowly due to a lower driving pressure than for the water. **Figure 12** illustrates how water and oil is distributed in

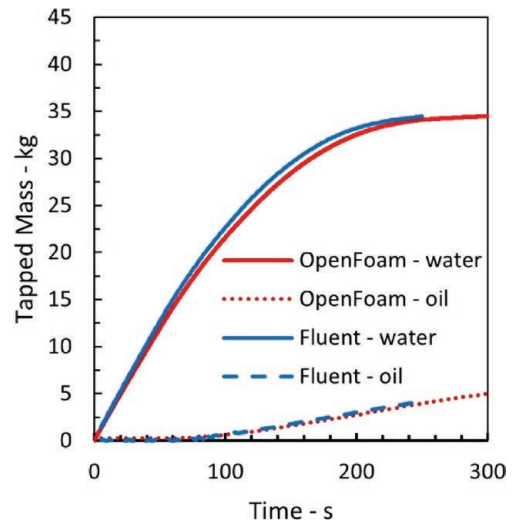


**Fig. 14.** Tapped mass of water and oil in tank with particles as function of time based on simulations. (Online version in color.)

the tank after 50 s, as oil is about to enter the tap-hole. We see that the interface between oil and water is even more severely deformed towards the tap-hole than was observed for the case without a particle bed (compare Figs. 7 and 12). Quantitatively, only the recording of total tapped mass was reported as a time series in the physical experiment due to the uncertainties involved in the image analysis for this case. This is shown in **Fig. 13** together with numerical results. The numerical simulations are consistent with the experimental recordings of total tapped weight of water and oil. Since the image analysis of height levels was not possible here, only a comparison between numerical results from the two software packages was possible for the individual tapping rates of the water and oil phases. This is shown in **Fig. 14**. The results from OpenFOAM and Ansys Fluent are consistent with each other, and show that tapping of oil starts 70 to 80 s after the tap-hole was opened.

## 5. Conclusions

A combined experimental and numerical study on tapping of two immiscible liquids from a vessel containing a particle bed was conducted. Oil and water were chosen as model liquids to be tapped out of a tank filled with spherical glass bead particles. Both OpenFOAM® and Ansys Fluent software were applied for CFD simulations. When comparing tapping rates from cases with and without a particle bed, it was seen that the particle bed exerts a significant resistance to the liquid flow and reduces the tapping rate appreciably. This was confirmed both by the physical experiments and the numerical simulations. When comparing the results on tapping from the tank without a particle bed, the numerical predictions deviated from the experimental results to a small degree. It was postulated that this is due to the models poorly capturing the pressure loss in the severely distorted flow at the tap-hole entrance. When a particle bed is present, the numerical simulations are consistent with the experimental results. This can be attributed to the fact that in the presence of a particle bed, the total pressure loss is dominated by the pressure loss through the particle bed, while the

tap-hole channel pressure loss is insignificant. It was also shown that the tapping rate was sensitive to the particle bed packing near to the tap-hole entrance. The proximity to a wall reduces the freedom to pack particles, and wall packing has to be accounted for in such processes. In conclusion, if wall packing (or other specifics of the particle packing close to the entrance of the tap-hole) is accounted for, and the tap-hole channel pressure loss is insignificant, numerical CFD models of the problem generally perform well.

Of course, the prediction of tapping rates from real ferroalloy smelting furnaces is a considerably more challenging problem. It is difficult to properly assess the packing of coke and ore close the entrance of the tap-hole during a given tap, and the numerical predictions are sensitive to this detail. Future efforts should therefore focus not only on model development but also on characterizing the particle bed close to the tap-hole. Numerical models can also be calibrated against observations of data such as tap masses and tapping rates, which could then be applied in inverse modelling to obtain information about the particle packing. In retrospect some more work on the lighting conditions should have been carried out to improve observations of individual tapping of water and oil in a particle bed.

#### Acknowledgement

This paper is published by permission of Mintek, SINTEF and NTNU. The authors acknowledge the Research Council of Norway and The Norwegian Ferroalloy Producers Research Association for providing funding through the projects Controlled Tapping (project code 10092390) and Recursive (project code 326581), and the Centre for High Performance Computing (CHPC), South Africa, for providing computational resources to this research project.

#### Conflict of Interest

The authors declare no conflicts of interest.

#### Nomenclature

- $g$ : Acceleration of gravity ( $\text{m/s}^2$ )
- $p$ : Pressure (Pa)
- $S$ : Momentum source term ( $\text{kg/m}^2\text{s}^2$ )
- $t$ : Time (s)
- $U$ : Superficial velocity (m/s)

#### Greek

- $\alpha$ : Volume fraction (-)
- $\epsilon$ : Particle bed porosity (-)
- $\rho$ : Density ( $\text{kg/m}^3$ )

#### Subscripts

- $i$ : Fluid phase index

#### REFERENCES

- 1) L. R. Nelson and R. Hundermark: *J. South. Afr. Inst. Min. Metall.*, **116** (2016), 465. [http://www.scielo.org.za/scielo.php?script=sci\\_arttext&pid=S2225-62532016000500014&lng=en&nrm=iso](http://www.scielo.org.za/scielo.php?script=sci_arttext&pid=S2225-62532016000500014&lng=en&nrm=iso), (accessed 2023-10-20).
- 2) J. D. Steenkamp, J. J. Sutherland, D. A. Hayman and J. Muller: *JOM*, **68** (2016), 1547. <https://doi.org/10.1007/s11837-016-1862-9>
- 3) S. Olsen, M. Tangstad and T. Lindstad: Production of Manganese Ferroalloys, Tapir Academic Press, Trondheim, (2007), 247.
- 4) J. E. Olsen: Proc. 16th International Ferro-Alloys Congress (INFA-CON XVI) 2021, SSRN, (2021). <https://doi.org/10.2139/ssrn.3926099>
- 5) J. C. Parker: *Rev. Geophys.*, **27** (1989), 311. <https://doi.org/10.1029/RG027i003p00311>
- 6) Y. Yan, L. Wang, T. Wang, X. Wang, Y. Hu and Q. Duan: *Flow Meas. Instrum.*, **60** (2018), 30. <https://doi.org/10.1016/j.flowmeasinst.2018.02.017>
- 7) T. Fukutake and K. Okabe: *Trans. Iron Steel Inst. Jpn.*, **16** (1976), 309. <https://doi.org/10.2355/isijinternational1966.16.309>
- 8) M. J. Luomala, O. J. Matilla and J. J. Härkki: *Scand. J. Metall.*, **30** (2001), 225. <https://doi.org/10.1034/j.1600-0692.2001.300405.x>
- 9) M. Vångö, S. Pirker and T. Lichtenegger: *Appl. Math. Model.*, **56** (2018), 501. <https://doi.org/10.1016/j.apm.2017.12.008>
- 10) J. Liang, Y. Ma and Y. Zheng: *Theor. Appl. Mech. Lett.*, **11** (2021), 100300. <https://doi.org/10.1016/j.taml.2021.100300>
- 11) J. Zhang, F. Larachi and S. M. Taghavi: *Ind. Eng. Chem. Res.*, **60** (2021), 1452. <https://doi.org/10.1021/acs.iecr.0c05343>
- 12) W. B. U. Tanzil, P. Zulli, J. M. Burgess and W. V. Pinczewski: *Trans. Iron Steel Inst. Jpn.*, **24** (1984), 197. <https://doi.org/10.2355/isijinternational1966.24.197>
- 13) W. Liu, L. Shao and H. Saxén: *Metals*, **10** (2020), 496. <https://doi.org/10.3390/met10040496>
- 14) Q. He, P. Zulli, G. M. Evans and F. Tanzil: *Asia-Pac. J. Chem. Eng.*, **14** (2006), 249. <https://doi.org/10.1002/apj.5500140122>
- 15) T. Nouchi, M. Yasui and K. Takeda: *ISIJ Int.*, **43** (2003), 175. <https://doi.org/10.2355/isijinternational.43.175>
- 16) V. Loomba, H. Pourfallah, J. E. Olsen and K. E. Einarsrud: Proc. Furnace Tapping 2022, The Minerals, Metals & Materials Series, Springer, Cham, (2022), 159. [https://doi.org/10.1007/978-3-030-92544-4\\_13](https://doi.org/10.1007/978-3-030-92544-4_13)
- 17) K. Nishioka, T. Maeda and M. Shimizu: *ISIJ Int.*, **45** (2005), 669. <https://doi.org/10.2355/isijinternational.45.669>
- 18) V. Loomba, J. E. Olsen and K. E. Einarsrud: Proc. Furnace Tapping 2022, Minerals, Metals & Materials Series, Springer, Cham, (2022), 325. [https://doi.org/10.1007/978-3-030-92544-4\\_24](https://doi.org/10.1007/978-3-030-92544-4_24)
- 19) M. Kadhodabeigi, H. Tveit and S. T. Johansen: *ISIJ Int.*, **51** (2011), 193. <https://doi.org/10.2355/isijinternational.51.193>
- 20) M. Iida, K. Ogura and T. Hakone: *ISIJ Int.*, **48** (2008), 412. <https://doi.org/10.2355/isijinternational.48.412>
- 21) L. Shao and H. Saxén: *ISIJ Int.*, **51** (2011), 228. <https://doi.org/10.2355/isijinternational.51.228>
- 22) D. A. Drew and S. L. Passman: Theory of Multicomponent Fluids, Springer, New York, (1999), 308.
- 23) J. E. Olsen and Q. G. Reynolds: *Metall. Mater. Trans. B*, **51** (2020), 1750. <https://doi.org/10.1007/s11663-020-01873-1>
- 24) S. Bublik, J. E. Olsen, V. Loomba, Q. G. Reynolds and K. E. Einarsrud: *Metall. Mater. Trans. B*, **52** (2021), 2038. <https://doi.org/10.1007/s11663-021-02134-5>
- 25) Z. H. Guo, Z. Sun, N. Zhang, M. Ding and X. Cao: *Powder Technol.*, **319** (2017), 445. <https://doi.org/10.1016/j.powtec.2017.06.061>
- 26) A. de Klerk: *AIChE J.*, **49** (2003), 2022. <https://doi.org/10.1002/aic.690490812>
- 27) C. W. Hirt and B. D. Nichols: *J. Comput. Phys.*, **39** (1981), 201. [https://doi.org/10.1016/0021-9991\(81\)90145-5](https://doi.org/10.1016/0021-9991(81)90145-5)
- 28) S. Ergun: *Chem. Eng. Prog.*, **48** (1952), 89.
- 29) OpenFOAM v2206, ESI, Bracknell, (2022), <https://www.openfoam.com/news/main-news/openfoam-v2206>, (accessed 2022-09-20).
- 30) porousInter, O. F. Oxtoby, Cape Town, (2022), <https://gitlab.com/opensimproject/porousinter>, (accessed 2022-09-20).
- 31) O. Oxtoby, J. Heyns and R. Suliman: Proc. Open Source CFD Int. Conf., (Hamburg), (2013). <https://doi.org/10.13140/2.1.3075.8400>